ISSN 0031-918X, Physics of Metals and Metallography, 2020, Vol. 121, No. 7, pp. 701–707. © Pleiades Publishing, Ltd., 2020.
Published in Russian in Fizika Metallov i Metallovedenie, 2020, Vol. 121, No. 7, pp. 771–778.

STRENGTH AND PLASTICITY

Studying the Structure of Al–Mg–Si Casting Alloys Doped by Lithium

O. Trudonoshyn[a, b, *]

[a] *Vyatskiy State University, Department of Materials Science and Design Basics, Kirov, Moscow, 610000 Russia*
[b] *Friedrich-Alexander-Universität Erlangen-Nürnberg, Materials Science Department, Erlangen, 91058 Germany*
**e-mail: oltrud@gmail.com*

Received January 15, 2020; revised February 18, 2020; accepted February 25, 2020

Abstract—The article discusses changes in the structure of Al–Mg–Si cast alloys after their additional alloying with lithium. To predict and explain the phase transformations in the studied alloys, phase diagrams were calculated using Thermo-Calc software. Thermo-Calc results are in good agreement with microstructure analysis. The morphology and chemical composition of the intermetallic phases were studied using a scanning electron microscope and EDX analysis on polished and deeply etched microsections. There were revealed several intermetallic phases in the studied alloys. It was found that the addition of lithium has a modifying effect on the structure of the studied alloys, which also leads to the formation of a new AlLiSi phase. To analyze the effect of lithium on the mechanical properties, the Brinell hardness, tensile strength, yield strength, and elongation were measured. Additional alloying with lithium leads to an increase in the strength properties of the studied alloys compared to the base alloy.

Keywords: Al–Mg–Si alloys, lithium, microstructure, phase diagrams

DOI: 10.1134/S0031918X2007011X

INTRODUCTION

The development of aluminum alloys goes hand in hand with the developments in the aircraft industry. From the 1920s to the present time aluminum alloys have been the basic materials for aircraft frames [1–3]. The attractiveness of aluminum alloys is based on their relative cheapness, high corrosion resistance, thermal conductivity, and low coefficient of thermal expansion. In addition, aluminum alloys have an excellent strength-to-weight ratio. Aluminum alloys are those of the most easily manufactured among all high-performance materials, since parts from them can be obtained by all known foundry technologies [1, 4].

Al–Si system is the most popular among all aluminum alloys. The mechanical properties of the Al–Si alloys depend not only on the alloy composition, but also on the microstructure features, such as the size and the morphology of aluminum dendrites, eutectic silicon, and other intermetallic phases [4, 5]. Microalloying of the casting Al alloys with the aim of changing the morphology of the phases is an effective way to increase the mechanical properties (especially elongation). The modifying effect of strontium on the eutectic silicon [5, 6] is the most studied. However, it was reported in the work [5] that Li also has a modifying effect on the morphology of the structural components of the Al–8.5% Si–3.5% Cu–1% Fe alloy. The changes in the structure lead to an increase in strength by 10% and elongation by more than 30%, compared with the base alloy.

There is a great demand in the aircraft materials market for the low-density aluminum alloys in searching for the solution of reducing fuel consumption. The alloying with lithium leads to a synergistic effect, since the addition of each 1 wt.% Li reduces the density of the alloy by 3% and increases Young's modulus by 6% [7–9]. At present, third-generation Al–Li alloys are widely used. The most of the alloys belong to the Al–Cu–Li–Mg system. However, increasing the copper content and lowering the magnesium content in the alloys from generation to generation leads to a lowering of the lithium effect on the density of alloys. Thus, the average density of Al–Li alloys of the third generation is about 2.7 g/cm^3, while of the first is 2.47 g/cm^3 [3, 10]. In this context, casting alloys of the Al–Mg–Si system or wrought alloys of the 6000 series might be extremely useful [10, 11]. Alloys of this system have a perfect strength-ductility ratio. Wrought alloys of this system are widely used in the automotive and aerospace industries, while cast ones remain underestimated [12]. Lithium has a relatively high solubility in aluminum. Thus, the artificial aging of the Al–Mg–

Table 1. Alloys composition, wt %

Alloy	Mg	Si	Mn	Li
M (base)	5.5	2.5	0.6	–
L1	5.5	2.5	0.6	1.0
L2	3.0	2.5	0.6	1.0

Si–Li alloys leads to the formation of at least two types of hardening precipitates: δ'-Al_3Li and β''-Mg_2Si. This fact makes it possible to obtain a new series of age-hardenable alloys with a lower weight density [12–14]. Similarly to the situation with cast Al–Mg–Si alloys, the effect of lithium is better studied on alloys of the 6000 series [8, 10, 15–19]. The effect of lithium on the structure and properties of the casting Al–Mg–Si alloys was reported for hypereutectic Al–15% Mg_2Si [20–22] and hypoeutectic Al–6% Mg_2Si [14, 23, 24] alloys (both alloys belong to the quasi-binary Al–Mg_2Si section). This work is the continuation of the study of the lithium effect on the hypoeutectic alloys [14, 24], yet, with that, it shifts emphasis from the quasi-binary Al–Mg_2Si section to the alloys with the ratio Mg : Si < 2.

MATERIALS AND METHODS

Casting hypoeutectic Al–Mg–Si alloys were chosen for additional alloying by Li. Their chemical composition is presented in Table 1. A resistance furnace with a graphite crucible was used for the melt preparation (melting weight 0.25 kg). High-purity aluminum (99.997) and master alloys AlSi25, AlMn26, AlMg50, and AlLi5 were used as starting materials. The melt with a temperature of 720 ± 5°C had been degassed under an argon atmosphere for 10 minutes. The molten metal was cast into a steel rectangular chill mold with a temperature of 20°C. Under these conditions, the cooling rate was 5 K s^{-1}. An Al–5.5Mg–2.5Si–0.6Mn commercial casting alloy was selected as a reference alloy.

The castings have dimensions 160 × 25 × 20 mm and weight about 250 g. Cubic samples with the size 10 × 10 × 10 mm were cut from the centre of the castings for the metallographic studies. Samples were prepared using standard metallographic procedures.

To visualize the morphology of the alloy structure, samples were etched in a 15% NaOH solution. The phase composition was measured using SEM EDX (JEOL JSM-6510 LV Japan with EDS analysers Oxford) with accelerating voltage of 15 kV.

Thermo-Calc, a commercially available software package used to perform thermodynamic and phase diagram calculations for multicomponent systems (Al–Mg–Si–Mn and Al–Mg–Si–Mn–Li), was employed to investigate the possible effects of alloying elements on the equilibrium phases in the alloy, using the TCAl2:Al-alloys v2.1 database.

RESULTS AND DISCUSSION

Analysis of the phase diagrams. A detailed analysis of the diagrams of the studied system is presented in [12]. Figure 1 shows multicomponent polythermal phase diagrams in the sections Al–*x*Mg–2.5Si–0.6Mn (for the base alloy M) and Al–*x*Mg–2.5Si–0.6Mn–1Li (for the studied alloys) to understand the phase formation in the studied alloys.

The diagram in Fig. 1a can be divided into 3 principal areas: (1) with excess silicon content, (2) with Mg : Si ratio close to the quasi-binary section; (3) with excess magnesium content. In the region with excess silicon, α-Al crystallizes as the primary phase, followed by crystallization of the α-AlMnFeSi phase and then β-Mg_2Si. The last formed phase in the region with an excess of silicon is the δ-AlMnFeSi phase. It is known from the literature that this phase has acicular morphology and is brittle, which leads to a significant decrease in the mechanical properties of Al–Mg–Si alloys in the as-cast state [25]. When the magnesium content is in the range of 3–3.5%, the alloys have the following set of phases: α-Al + α-AlMnFeSi + β-Mg_2Si. The harmful δ-AlMnFeSi phase is no longer formed. With a further increase in the magnesium content, the β-AlMg phase is formed. The α-AlMnFeSi phase crystallizes as primary, followed by α-Al, β-Mg_2Si. The β-AlMg phase precipitates already in the solid state. High cooling rates reduce the diffusion rate and impede the formation and growth of the phase [12].

In the system with 1% lithium, 3 new lithium-containing phases are formed: AlLiSi; δ-AlLi (in the region of the quasi-binary section); AlLiMg (in the area with excess magnesium). Moreover, the regions of existence of metastable δ-AlMnFeSi and β-AlMg phases are substantially narrowed. The addition of lithium does not significantly affect the equilibrium of the α-Al and α-AlMnFeSi phases.

The studied lithium-containing alloys belong to two zones: L1 alloy has magnesium and silicon content similar to the base alloy M, and belongs to the region with the stable phases α-AlMnFeSi, α-Al, and β-Mg_2Si; L2 alloy has excess silicon (due to the lower magnesium content) and is in the region of existence of the AlLiSi phase.

Microstructure analysis. The results of the Thermo-Calc calculations are in good agreement with the microstructural analysis of the studied alloys. The base alloy M (Fig. 2a–2c) consists of α-Al-dendrites, eutectic Al–Mg_2Si, and α-AlMnFeSi intermetallic phase. Similarly to the results reported in [12], the β-AlMg phase was not found in the structure. As can

be seen from the analysis of non-etched microsections (Figs. 2a, 2d), the structure of the L1 alloy does not significantly differ from the structure of the base alloy and consists of similar phases. The structure of the L2 alloy additionally has one new phase—the AlLiSi phase. Phases that precipitate at low temperatures (AlLiMg, AlLi) were not detected similarly to the β-AlMg phase.

It is clearly seen in Fig. 2b–2c (on deeply etched samples) that the Al–Mg_2Si eutectic in the base alloy has lamellar morphology (a more detailed analysis of the structure of the Al–5Mg–2Si–Mn alloy is given in [24, 26]), while the eutectic in the L1 alloy has a fine fibre morphology. Table 2 shows the sizes and parameters of the microstructural components of the studied alloys.

It can be seen from Table 2 and Fig. 2 that the average size of eutectic colonies in the M and L1 alloys does not differ significantly. The size of the primary Mg_2Si crystals in the L1 alloy is also similar to that in the base alloy. However, the alloy additionally doped with lithium (L1) has a significantly lower size of the interlamellar (interfibrous) spacing. The morphology of primary crystals in hypoeutectic Al–Mg_2Si alloys was studied in detail in [24, 27], where it was found that octahedral primary crystals were thermodynamically more preferable. However, the addition of lithium leads to a change in the morphology of the primary crystals (Fig. 3). The modifying effect of lithium on the primary Mg_2Si crystals in hypereutectic Al–Mg_2Si alloys was also reported in [20–22].

In the L2 alloy, a decrease in the size of the eutectic colonies and the size of the primary Mg_2Si crystals is associated with a lower volume fraction of Mg_2Si in the alloy. Table 3 shows the volume fractions of the phases of the studied alloys calculated in the Thermo-Calc software.

Table 4 represents the EDX-analysis of α-Al dendrites, α-AlMnFeSi and AlLiSi intermetallic phases. As can be seen, Li does not affect the α-AlMnFeSi phase, and also does not significantly affect the solubility of elements in α-Al (alloy L1).

The concentration of magnesium in α-Al of the L2 alloy are two times lower than in the M and L1 alloys. This is due to the ratio of magnesium and silicon in the alloy ($Mg : Si_{L2} = 1.2$) and is in good agreement with the results of [25, 28].

The lithium-containing phase (AlLiSi) in the L2 alloy can be found in two forms: the morphology of compact, rounded phase, and in the a eutectic form (Fig. 4). The Al–AlLiSi eutectic consists of very thin (compared to Al–Mg_2Si eutectic) fibres (gray dotes) that alternate with Mg_2Si (black dotes) fibers, thus forming a triple Al–Mg_2Si–AlLiSi eutectic.

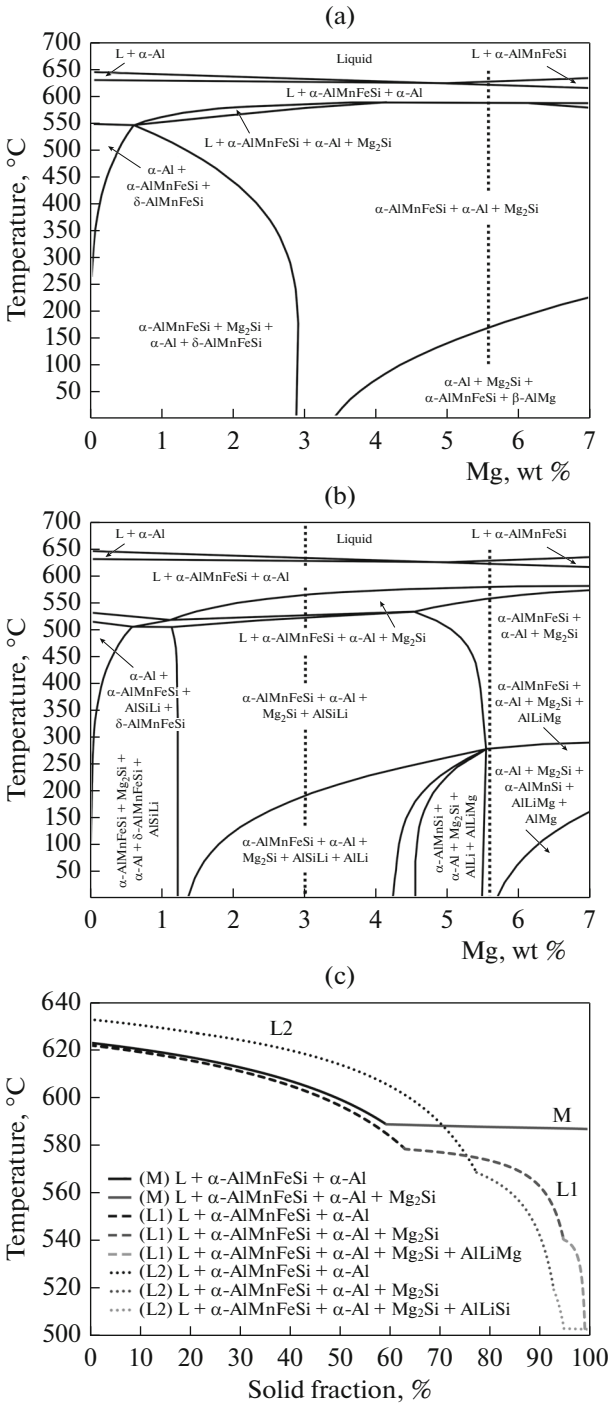

Fig. 1. Equilibrium phase diagrams at cross-sections: (a) Al–*x*Mg–2.5Si–0.6Mn; (b) Al–*x*Mg–2.5Si–0.6Mn–1.0–Li; (c) solidification curves of the studied alloys (d).

Mechanical properties. As it was reported in [12], casting alloys of the Al–Mg–Si system (unlike wrought series) cannot be hardened by precipitation hardening. This is due to the excess magnesium content (ratio Mg/Si > 2). On the other hand, the structure of the casting alloys with excess silicon [25, 28]

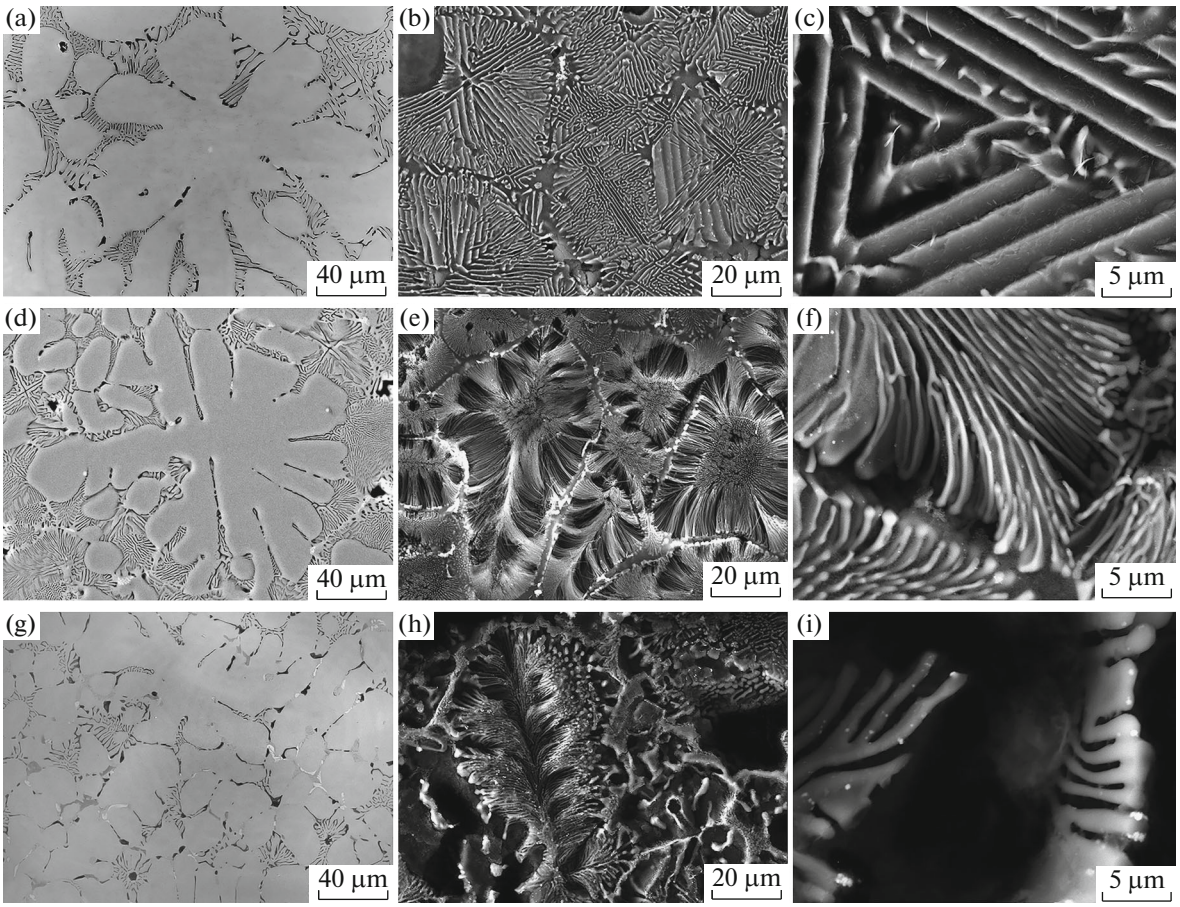

Fig. 2. Microstructures of the studied alloys: (a–c) base alloy M; (d–f) alloy L1; (g–i) alloy L2.

contains brittle needle-shaped silicides, which significantly reduce the mechanical properties of the alloys in the cast state. Thus, alloys with a ratio of 1.2 > Mg/Si > 1.5 in the as-cast state showed strength and hardness values 30–40% lower than that of alloys with a ratio of Mg/Si > 2.

In contrast to the results reported in [12, 25], the L2 alloy (Mg/Si = 1.2) has significantly higher prop-

Table 2. The parameters of the microstructural components of the studied alloys, μm

Parameters	M	L1	L2
Secondary dendrite arm spacing	25 ± 5	19 ± 7	15 ± 6
Interlamellar (interfibrous) spacing	2.1 ± 0.5	0.9 ± 0.4	1.1 ± 0.6
Size of eutectic colonies Al–Mg_2Si	36.8 ± 9.7	38 ± 12	12.7 ± 5.3
Size of the primary Mg_2Si crystals	9.1 ± 3.8	8.7 ± 1.9	4.5 ± 1.5

Table 3. Volume fractions of phases of the studied alloys (calculated in Thermo-Calc software, for a temperature of 300°C), %

Phase	M	L1	L2
α-Al	91.7	91.9	91.3
Mg_2Si	6.7	6.5	4.1
α-AlMnFeSi	1.6	1.6	1.6
AlLiSi	–	–	3.0

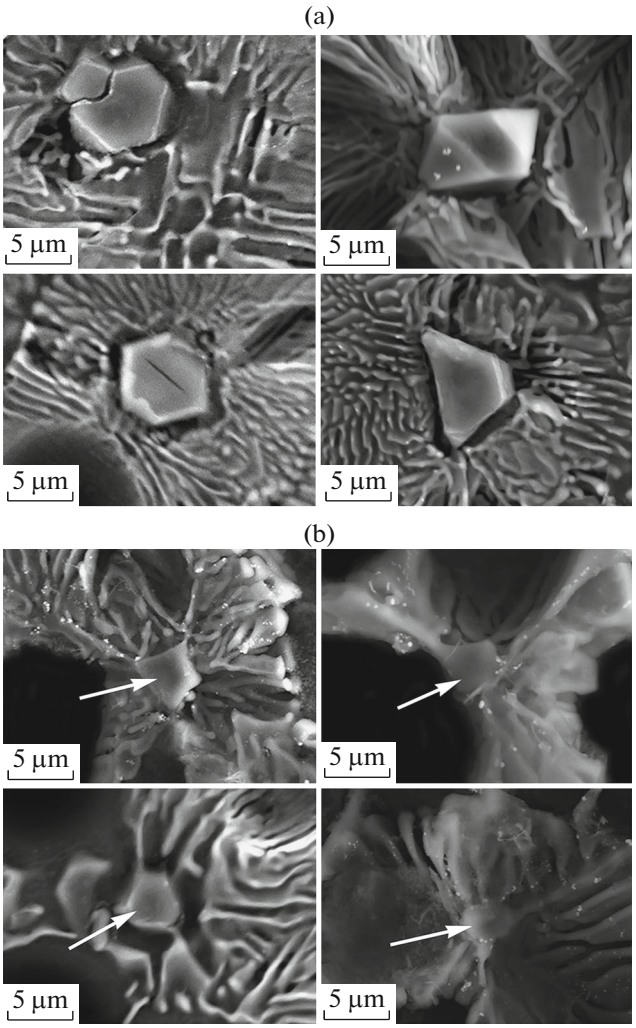

Fig. 3. Morphology of primary crystals in the studied alloys: (a) L1; (b) L2.

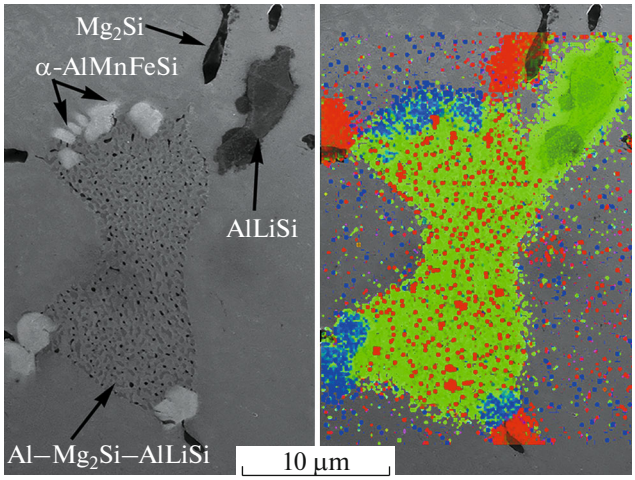

Fig. 4. Distribution of elements (red—Mg, green—Si, blue—Mn) in a triple eutectic Al–Mg_2Si–AlLiSi.

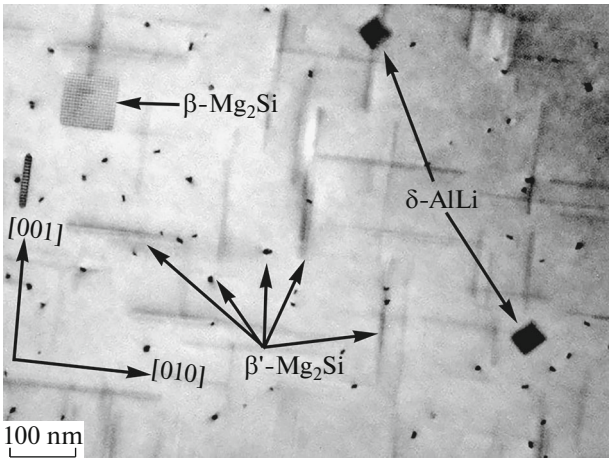

Fig. 5. TEM image of the structure of dendrite of the α-Al alloy doped by lithium after its artificial aging.

erties in the as-cast state compared to the L1 alloy (Mg/Si = 2.2) (Table 5). High values of the mechanical properties of the L2 alloy are associated with the absence of the brittle δ-AlMnFeSi phase in the alloy structure, which is the reason for the low properties in alloys with the ratio Mg/Si < 2. [25, 28]. In addition, the content of silicon and magnesium in the α-Al solid solution in the L2 alloy is close to the stoichiometric ratio of the Mg_2Si compound (Table 5). This promotes the formation of β" and β' nanosized precipitates in the α-Al solid solution [29, 30].

Moreover, the heat treatment of lithium-alloyed alloys has a significant effect on the mechanical properties, in contrast to the base alloy (Table 5). The artificial aging of lithium-containing alloys leads to the formation of δ-AlLi nano-sized precipitates in the alloy structure [14, 23], and, in addition, to the typical precipitates for this system β", β', and β (Fig. 5).

SUMMURY

(1) The structure of the base alloy consists of α-Al dendrites, α-AlMnFeSi intermetallic compounds, and Al–Mg_2Si eutectic. Primary Mg_2Si crystals were found in the center of the eutectic cells. The main hardening phase in the base alloy is the Al–Mg_2Si eutectic. α-AlMnFeSi intermetallic compounds are formed as a result of the addition of manganese to neutralize the negative effect of iron on ductility.

Table 4. EDX-analysis of the phases in the studied alloys, wt%

Alloy	Al	Mg	Si	Mn	Fe	Li
			α-Al			
M	97.0	2.3	0.3	0.4	0.1	–
L1	97.1	2.2	0.3	0.4	0.1	*
L2	97.9	1.2	0.5	0.4	0.1	*
			α-AlMnFeSi			
M	67.0	0.2	10.2	21.5	1.1	–
L1	65.5	0.7	9.0	22.7	2.1	–
L2	62.4	0.6	11.7	22.9	2.0	–
			AlLiSi			
L2	51.6	–	48.4	–	–	*
L2**	8.75	–	25.0	–	–	66.25

* Lithium cannot be detected by Oxford INCA Energy 250.
** Calculated by Thermo-Calc software program.

Table 5. Mechanical properties of the studied alloys

Alloy	Mg/Si	Condition	HB	σ, MPa	$\sigma_{0.2}$, MPa	δ, %
M	2.2	as-cast	79	225 ± 4	159 ± 4	6.7 ± 1.1
		HT	83	231 ± 4	165 ± 3	6.2 ± 1.4
L1	2.2	as-cast	91	241 ± 5	165 ± 3	7.1 ± 1.9
		HT	103	255 ± 5	175 ± 4	6.5 ± 2.0
L2	1.2	as-cast	110	272 ± 7	224 ± 5	6.1 ± 1.6
		HT	122	298 ± 9	238 ± 5	5.6 ± 1.1

HT: homogenization 60 min at 575°C, quenching in water, artificial aging 120 min at 175°C.

(2) The addition of 1% lithium to the base alloy does not lead to the formation of new phases, but it has a modifying effect. Thus, the eutectic morphology has changed from lamellar to fibrous. This effect leads to increasing the hardness and strength of the alloy in the as-cast state.

(3) The morphology of the eutectic colonies in the L2 alloy is similar to the L1 alloy, but, due to the lower volume fraction of Mg_2Si, the size of the colonies is smaller. Excess silicon in the system caused the formation of the AlLiSi phase, which is represented in the structure by two morphologies (primary compact, rounded phase and Al–Mg_2Si–AlLiSi triple eutectic).

(4) In the course of the artificial aging of alloys, several dispersed hardening phases (β'', β', β-Mg2Si) are formed in the structure of α-Al dendrites. Doping with lithium additionally leads to the release of the dispersed phase δ (AlLi).

REFERENCES

1. N. E. Prasad and R. J. H. Wanhill, *Aerospace Materials and Material Technologies. Vol. 1: Aerospace Materials* (Springer, Singapore, 2017).
2. I. N. Friedlander, "Modern aluminum and magnesium alloys and composite materials based on them," Met. Sci. Heat Treat. **44**, 24–29 (2002) [in Russian].
3. V. V. Antipov, N. A. Lavro, V. V. Sukhoivanenko, and O. G. Senatorova, "Experience in the use of Al–Li alloy 1441 and laminates based on it in seaplanes," Tsvetn. Met. **9**, 46–50 (2013) [in Russian].
4. E. L. Prach and K. V. Mikhalenkov, "Development of a new Al–Mg–Si–Mn system alloy with a Li addition" (Liteynoye Proizvodstvo [Foundry] **7**, 13–15 (2014) [in Russian].
5. M. Karamouz, M. Azarbarmas, and M. Emamy, "On the conjoint influence of heat treatment and lithium content on microstructure and mechanical properties of A380 aluminum alloy," Mater. Des. **59**, 377–382 (2014).
6. E. Ogris, A. Wahlen, H. Lüchinger, and P. J. Uggowitzer "On the silicon spheroidization in Al–Si alloys." J. Light Met. **2**, 263–269 (2002).
7. U. D. Shamas, B. A. Hasan, N. H. Tariq, and M. Mehmood, "Effect of Li addition on microstructure and mechanical properties of Al–Mg–Si alloy," Int. J. Mater. Res. **105**, 770–777 (2014).
8. U. D. Shamas, J. Kamran, N. H. Tariq, B. A. Hasan, R. H. Petrov, V. Bliznuk, and S. U. Zuha, "The synergistic effect of Li addition on microstructure, texture

and mechanical properties of extruded Al–Mg–Si alloys," Mater. Chem. Phys. **174**, 11–22 (2016).

9. L. G. Korshunov, L. I. Kaigorodova, N. L. Chernenko, and D. Yu. Rasposienko, "Tribological properties and structure of aluminum-lithium alloys," Phys. Met. Metallogr. **119**, 1236–1242 (2018).
10. X. Yang, B. Xiong, X. Li, L. Yan, Z. Li, Y. Zhang, H. Liu, S. Huang, H. Yan, and K. Wen, "Microstructural evolution and phase transformation of Al–Mg–Si alloy containing 3% Li during homogenization", in *Physics and Engineering of Metallic Materials*, 1st ed., Ed. by Y. Han (Springer Nature Singapore Pte Ltd, Singapore, 2019), pp. 411–417.
11. X. Ren, Y. Huang, and Y. Liu, "Effect of homogenization on microstructure and properties of Al–Mg–Si roll-casting sheet," Phys. Met. Metallogr. **119**, 789–796 (2018).
12. O. Trudonoshyn, S. Rehm, P. Randelzhofer, and C. Körner, "Improvement of the high-pressure die casting alloy Al–5.7Mg–2.6Si–0.7Mn with Zn addition," Mater. Charact. **158**, 109959 (2019).
13. T. Saito, E. A. Mørtsell, S. Wenner, C. D. Marioara, S. J. Andersen, J. Friis, K. Matsuda, and R. Holmestad, "Atomic structures of precipitates in Al–Mg–Si alloys with small additions of other elements," Adv. Eng. Mater. **20**, 1–18 (2018).
14. E. L. Prach, A. I. Trudonoshin, V. V. Boyko, and K. V. Mihalenkov, Development of new casting alloys of the system Al–Mg–Si–Mn with additions 1.0 ace. Li and 0.1 ace. Ti 0.1 ace. Zr, Metall Lit'e. Ukraine **8**, 17–23 (2014). [in Russian]
15. U. D. Shamas, J. Kamran, B. A. Hasan, N. H. Tariq, M. Mehmood, and M. Z. Shamas, "Effect of thermomechanical treatments and aging parameters on mechanical properties of Al–Mg–Si alloy containing 3 wt % Li," Mater. Des. **64**, 366–373 (2014).
16. L. Yan, Y. Zhangn, X. Li, Z. Li, F. Wang, H. Liu, and B. Xiong, "Effect of Zn addition on microstructure and mechanical properties of an Al–Mg–Si alloy," Prog. Nat. Sci.: Mater. Int. **3**, 1–4 (2014).
17. E. A. Mørtsell, C. D. Marioara, S. J. Andersen, I. G. Ringdalen, J. Friis, S. Wenner, J. Røyset, O. Reiso, and R. Holmestad, "The effects and behaviour of Li and Cu alloying agents in lean Al–Mg–Si alloys," J. Alloys Compd. **699**, 235–242 (2017).
18. Y. Koshino, M. Kozuka, S. Hirosawa, and Y. Aruga, "Comparative and complementary characterization of precipitate microstructures in Al–Mg–Si(–Li) alloys by transmission electron microscopy, energy dispersive X-ray spectroscopy and atom probe tomography," J. Alloys Compd. **622**, 765–770 (2015).
19. R. Chen, Z. Huang, C. Q. Chen, J. Y. Shen, and Y. G. Zhang, "Thermodynamic calculated and TEM observed microstructure of Al–Li–Mg–Si alloys," Mater. Sci. Eng., A **280**, 146–150 (2000).
20. A. Razaghian, A. Bahrami, and M. Emamy, "The influence of Li on the tensile properties of extruded in situ Al–15% Mg_2Si composite," Mater. Sci. Eng., A **532**, 346–353 (2012).
21. R. Hadian, M. Emamy, and J. Campbell, "Modification of cast Al–Mg_2Si metal matrix composite by Li," Metall. Mater. Trans. B **40**, 822–832 (2009).
22. R. Hadian, M. Emamy, N. Varahram, and N. Nemati "The effect of Li on the tensile properties of cast Al–Mg_2Si metal matrix composite," Mater. Sci. Eng., A **490**, 250–257 (2008).
23. O. Prach, J. Hornik, and K. Mykhalenkov, "Effect of the addition of Li on the structure and mechanical properties of hypoeutectic Al–Mg_2Si alloys," Acta Polytech. **55**, 253–259 (2015).
24. O. Trudonoshyn, O. Prach, V. Boyko, M. Puchnin, and K. Mykhalenkov, "Design of a new casting alloys containing Li or Ti + Zr and optimization of its heat treatment," *Met. 2014 – 23rd Int. Conf. Metall. Mater. Conf. Proc.* (2014), pp. 1399–1404.
25. O. Prach, O. Trudonoshyn, and M. Puchnin, "Effects of chemical composition on mechanical properties of Al–Mg–Si–Mn based alloys," Mater. Eng. – Mater. Inžinierstvo **24**, 11–20 (2017).
26. O. Trudonoshyn, M. Puchnin, and K. Mykhalenkov "Features of structure formation and changes in the mechanical properties of cast Al–Mg–Si–Mn alloy with the addition of (Ti + Zr)," Acta Polytech. **55**, 282–290 (2015).
27. A. I. Trudonoshin and K. V Mihalenkov, "Morphology and properties of primary Mg_2Si crystals in alloys of Al–Mg–Si system," Cast. Processes **5**, 38–47 (2014) [in Russian].
28. O. B. Berdova-Bashura, E. L. Prach, A. I. Trudonoshin, and K. V Mihalenkov, "Effect of chemical composition on structure and mechanical properties of Al-Mg-Si alloys," Cast. Processes **1**, 59–69 (2015) [in Russian].
29. C. D. Marioara, S. J. Andersen, J. Jansen, and H. W. Zandbergen "Atomic model for GP-zones in a 6082 Al–Mg–Si system," Acta Mater. **49**, 321–328 (2001).
30. S. J. Andersen, H. W. Zandbergen, J. Jansen, C. Træholt, U. Tundal, and O. Reiso "The crystal structure of the β" phase in Al–Mg–Si alloys," Acta Mater. **46**, 3283–3298 (1998).